MAUNEY, DANIEL T., M.S. New Instrument for Probing the Pure Rotational Spectroscopy of Cold Molecules Produced via “Billiard-like” Scattering. (2012) Directed by Dr. Liam Duffy. 52 pp.

Laser cooling of molecules has proved problematic due to their complex internal structure. Several alternative methods have been developed to cool molecules into the same temperature ranges previously attained using laser cooling methods on atoms. One of these methods is the “Billiard-like” scattering method developed by Elioff and coworkers at Sandia National Labs, which is attempted in this work.

A crossed molecular beam instrument was constructed, expanding the capabilities of the Duffy lab into crossed molecular beam studies, including the “Billiard-like” scattering method. This instrument included two differentially pumped “arms” to house molecular beam nozzles, gas inlet system, chopper, and a pulse sequence to reduce the systematic error associated with stagnation pressure drift and to adjust nozzle timing based on drifts in chopper speed. To accommodate the use of additional oscilloscopes with the pulse sequence, the main acquisition program was modified and a database was created for cataloging and searching past scans.

Based on the scans taken during this work, a preliminary rotational state changing collision cross-section was estimated.

# NEW INSTRUMENT FOR PROBING THE PURE ROTATIONAL SPECTROSCOPY OF COLD MOLECULES PRODUCED VIA "BILLIARD-LIKE" SCATTERING

by

Daniel T. Mauney

A Thesis Submitted to
the Faculty of the Graduate School at
The University of North Carolina at Greensboro
in Partial Fulfillment
of the Requirements for the Degree
Master of Science

Greensboro
2012

Approved by

_____
Committee Chair

APPROVAL PAGE

This thesis has been approved by the following committee of the Faculty of The Graduate School at The University of North Carolina at Greensboro.

Committee Chair_____

Committee Members_____

_____

_____
Date of Acceptance by Committee

_____
Date of Final Oral Examination

ACKNOWLEDGEMENTS

I would like to thank Dr. Liam Duffy for serving as my research advisor. Thank you for your patience, understanding, and guidance.

I would like to thank Dr. Alice Haddy and Dr. Solomon Bililign for agreeing to serve on my thesis committee.

I would like to thank Nicholas Mark and Josué Monge for their friendship and collaboration during the course of this work.

TABLE OF CONTENTS

Page

Page

LIST OF TABLES

Page

LIST OF FIGURES

Page

# CHAPTER I

# INTRODUCTION

## I.A. Background

The study of cold atoms and molecules at one point in the past 30 years was thought of as a passing "fad" in the scientific community, but has since blossomed into a growing field that promises to offer insight into fundamentally new areas of physics. One of these phenomena is the instantaneous dipole moment of an electron predicted by the standard model of particle physics. Despite its tiny size, the charge distribution of the electron itself is not localized around a single point; it is distorted. In a cold molecule, it may be possible to see the effects of this delocalization with ultrahigh resolution spectroscopy, although to date, it has never been measured. Current experiments are now within reach of testing some competing theoretical models within the standard model of particle physics. Successful measurement would, at a minimum, rule out some of these models.

Another phenomenon is related to a subtle quantum mechanical difference between chiral species. On the scale of fundamental particles, two left-handed fermions are the only ones to experience the weak interaction, one of the four fundamental forces in nature, showing that the universe leans towards left-handedness. This parity is not shown in any of the other fundamental forces. [1] Well known to chemists, left and

right handed enantiomers are currently very difficult to separate and are found in many different places in nature. For instance, all of the amino acids inside the human body are left handed and this purity is currently unexplained by current theories. The ability to study these molecules in a cold state may allow the subtle differences between this handedness to be accentuated. [2]

In recent years, cold molecules have been used to create a new state of matter that was previously theorized by Albert Einstein and Satyendra Bose. This state of matter, called a Bose-Einstein Condensate (BEC), is created by trapping and cooling atoms to a density and temperature where the atomic spacing is smaller than their thermal de Broglie wavelength. By doing this, it forces the atoms into their lowest possible ground state, creating a macroscopic quantum object from a diffusion cloud of ultracold gas. [3]

Currently, cold atoms are the basis of the world's most precise time standards, and as such, are used in the operation of Global Positioning Satellite systems, each having its own onboard atomic clock. These clocks are based on the decay of laser cooled $^{133}$Cs between two electronic states. The lifetime of the upper states is known to a very precise degree and the length of a second is the time it takes to cycle $9.19 \times 10^{10}$ times between the two states, according to the International System of Units. Better methods of cooling could allow an even more precise measurement of this transition and hence a more precise clock. [2]

Some of the other uses for cold molecules include increasing the interaction time between molecules and light leading to ultra-high resolution spectroscopic methods [4], reaction mechanisms that in a cold state could "tunnel" through activation energy

barriers, the ability to measure the lifetime of transient and intermediate species [5], and the possibility of using trapped atom and molecules as the basis of a new form of computing [6]. It is the purpose of the work here to i) generate cold $N_2O$ molecules by imitating the method of Elioff et al. [7] using molecule-molecule "Billiard-like" scattering, ii) measure their translational temperature via Doppler spectroscopy, and iii) to determine the cross-section of the collision through rotational absorption line intensities. The application of millimeter wavelength spectroscopy to such crossed molecular beams experiments is new, affording ultrahigh resolution and hyperfine detail.

## I.B. History of Cold Atoms and Molecules

In cold molecule research, for an atom or molecule to be cold, it must possess a translational temperature less than 1 K or a thermal de Broglie wavelength on the order of its classical size. [5] In 1905, Albert Einstein published four papers, one of which being "On a Heuristic Viewpoint Concerning the Production and Transformation of Light" in which he theorized that light travelled in discrete packets that he called photons. [8] This was demonstrated in 1914 when Robert Milliken showed that the energy of ejected electrons increased linearly with frequency and not with intensity. [9] This was a key step in showing the wave-particle duality of light. In 1924, Louis de Broglie, as part of his Ph.D. thesis for the University of Paris, theorized that the wave-particle duality of light could also be expanded to include all particles and the wavelength of such particles is inversely proportional to their momentum. [10] The thermal de Broglie wavelength, $\lambda$,

is approximately equal to the average of the individual de Broglie wavelengths of the particles at a given temperature and can be expressed as:

$$\lambda = \frac{h}{\sqrt{2\pi m k_B T}} \tag{1.1}$$

where h is Planck's constant, m is the mass of the particle, $k_B$ is Boltzmann's constant and T is the temperature. [11]

Theories for the cooling of atoms first appeared in the mid 1970's with the development of laser cooling techniques. These techniques took advantage of the force that light exerts on particles. This is a result of the momentum of a photon as it is absorbed/scattered from an atom or molecule. This is dramatically demonstrated in the tails of comets where the tail always points away from the sun!

In 1933, Frisch demonstrated that the light from a Na lamp could broaden a narrow beam of sodium atoms. [12] Later, with the development of the laser, Piqué and Vialle [13] were able to deflect sodium and cesium with a dye laser, thereby expanding the work of Frisch.

Based on the success of early experiments, researchers began developing experiments to slow molecules by aiming a laser that is slightly Doppler detuned below a transition frequency directly into the path of an oncoming atomic beam. When the atoms in the gas absorb the incoming light, they slow down due to the momentum of the incoming light being in the opposite direction of the atom's travel. When the atoms subsequently relax through spontaneous emission, the emitted photons then "push" the

particle in random directions. This recoil from emission is the reason for the lower temperature limit of laser cooling alone. Over the course of the path, each particle in the gas would absorb and emit many times, cooling the beam substantially. This theory was proposed simultaneously by Hänsch and Shawlow at Stanford University [14] and Wineland and Dehmelt from the National Bureau of Standards in Boulder, Colorado. [15] The first attempts were performed using trapped ions of magnesium by irradiating with 8 μW from a dye laser. This method was shown to "cool" the gas below 40 K. [16] Later, this technique was refined and expanded to the cooling of neutral atoms. [17]

The laser cooling of atoms is much simpler than laser cooling of molecules due to the complex internal structure of molecules and hence a myriad of spectroscopic transitions. As a result, the repeated cycling of a single electronic transition is not possible for molecules because the fluorescence does not return the molecule to the original quantum state. The main reason for this is due to overlapping electronic states and their corresponding vibrational wave functions that allow for a molecule to relax into multiple vibrational levels. [2] This complexity makes it very difficult to cool molecules using the same methods used with atoms, and therefore new techniques are needed to cool molecules to the same degree.

## I.C. Methods for Cooling Molecules

Some methods that have been developed to cool molecules include: photoassociation, buffer-gas loading, feshbach resonance, Stark deceleration, and crossed beam elastic/inelastic scattering. In photoassociation cooling, two atoms that were

previously cooled in a magneto-optical trap are bombarded by light from another laser resonant with a dimer transition. These atoms then absorb a photon jointly to become bound in an excited state. The excited state lifetime of these dimers is very short and often the atoms will emit the absorbed photon and fall back into the dimer ground state. [18] [19] This method has been demonstrated with atoms as small as hydrogen and as large as ytterbium and has shown the ability to cool dimers into the ultracold regime with a translational temperature below 1 mK. [20]

Buffer-gas loading is a technique wherein paramagnetic atoms or molecules are trapped within a magnetic trap along with a paramagnetic buffer-gas. The buffer gas, usually helium, will collide with the molecule of interest, transferring some of the momentum from the molecule to the helium. The "warmed" helium is then allowed to escape, leaving the net translational temperature of the remaining molecules lower than the original sample. This method was developed by Frank C. De Lucia at Duke University in 1984 [21] and was shown by Doyle et al. at Harvard University [22] and other groups to cool molecules in the mK range.

Feshbach resonance cooling involves colliding two atoms or molecules so that the collision energy is degenerate with a bound state. These dimers are then trapped and subjected to a magnetic field ramp that slowly cools the dimers. This method, as with photoassociation, can cool these dimers into the ultracold regime. [23] Stark deceleration, sometimes called sisyphus cooling, uses a series of electric fields. Polar molecules are forced to climb a series of potential gradients, which are a function of the molecule's Stark energy in the applied field. These gradients slowly bring them to a stop. This

method has been shown to cool CO molecules into the micro-kelvin range by Gerard Meijer's group at the Max Planck Institute in Berlin. [24]

The method used in this work is termed "Billiard-like" scattering as coined by David Chandler at Sandia National Labs. [25] His method involves colliding atoms or molecules in such a way that the translational energy of one is transferred to the other, leaving one with very minimal translational energy in the laboratory frame of reference. Since the cooling is due to a single collision event, the experimental setup also affords the ability to study the cross section of the scattering. The larger the cross-section, the more likely they are to collide.

## I.D. Collision Theory

### I.D.1. Cross-Section

To mathematically define a collisional cross-section, it is necessary to define the effective collision radius, d. Since molecular shape can be complex and varies from molecule to molecule and with collision energy, it will be simpler to consider each molecule as a hard sphere. This hard sphere will have a radius defined as r. The size of r is dependent on the range of the electrostatic forces between the colliding molecules. For example, as a polar LiCl collides with another LiCl it will feel repulsive or attractive forces depending on its orientation, which in turn changes its direction of travel and/or quantum state. In this case, each LiCl will have a very large effective radius and therefore a very large cross-section:

$$\sigma_{AB} = \pi d^2 \tag{1.2}$$

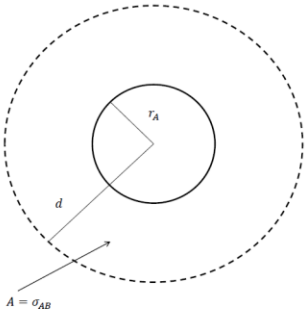


Figure 1**.** Visual representation of a simple hard-sphere cross-section

I.D.2. Newton Diagrams

When studying collisions, it is often necessary to convert from the laboratory frame of reference of the experimenter to the center-of-mass frame of reference of the molecules. This frame of reference relates the trajectory of the molecules in the beam relative to each other. If an observer were to ride on the center-of-mass, they would observe that each of the initial reactant beams would be moving toward the center-of-mass with a velocity that reflects the component of their laboratory frame velocities along the relative velocity axis of the collision, as shown by $\mathbf{u}_1$ and $\mathbf{u}_2$ in figure 2.

The transformation from the laboratory to the center-of-mass frame of reference is done using a Newton Diagram. [26]

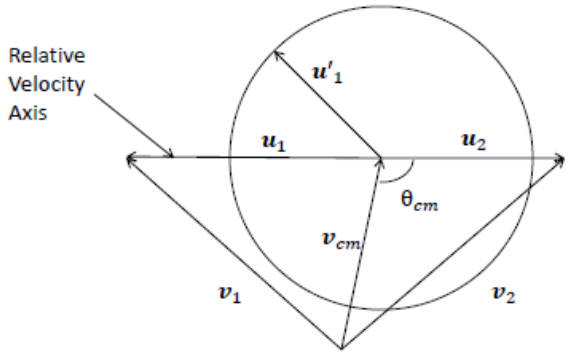


Figure 2. Sample newton diagram showing relative velocity axis and sample product trajectory. The circle is a 2D representation of the sphere of scattered products.

In this diagram, $v_1$ and $v_2$ represent the velocities of the colliding molecules in the laboratory frame, whereas $u_1$ and $u_2$ represent the molecule's relative velocity in the center-of-mass, and in the case of non-reactive scattering $u'_1$ represents the velocity after the collision of reactant 1. The center-of-mass velocity splits the angle between the two laboratory frame velocities.

When scattering occurs, the molecules will be ejected from the scattering region in random directions. These scattered molecules will form an expanding sphere around the center-of-mass. The "billiard-like" method for producing cold molecules works because a small fraction of these scattered molecules will have a velocity equal and opposite to the center-of-mass motion in the lab. Thus, this small subset of molecules will have near zero velocity in the laboratory frame.

## I.E. David Chandler's Experiment

### I.E.1. Molecular Beams

Chandler's experiment employs the use of molecular beams to add a measure of control to the scattering collision. A molecular beam is a grouping of molecules, in the gas phase, that move uniformly in one direction. This is achieved using various nozzles. The molecules initially are stagnant behind the nozzle opening at pressures anywhere from 1 torr to 1000 torr, and when the nozzle opens to a low pressure region, they stream out of the opening at a speed proportional to the difference in pressure between the two regions. If the pressure difference is great enough, their speed surpasses the speed of sound in that region, and is termed a supersonic expansion. [27]

There are types of nozzles named for the shape of their opening. A pinhole nozzle has a very small hole. This allows molecules to expand outward from the source three dimensionally, with most molecules moving along the beam axis away from the source. Likewise, as the name implies, a slit nozzle has a long narrow opening. The expansions from this source are two-dimensional in nature, producing a sheet of evenly distributed molecules.

As molecules expand from a nozzle, energy within each molecule is transferred from rotational and vibrational modes into translational motion. The drastic cooling that accompanies this transfer can cause gas clustering. For the same stagnation pressure (pressure behind the nozzle), it is known that the slit nozzles cluster more than pinhole nozzles because they produce higher densities with colder internal state distributions.

Clustering is often remedied using a carrier gas. As molecules escape the nozzle, they collide with and are diluted by the carrier gas, reducing the chance of clustering within the beam and providing a narrower velocity distribution.

### I.E.2. Experimental Setup

The setup employed by David Chandler's group at Sandia National labs uses two pinhole source nozzles that are fixed at a 90 degree angle. These nozzles are doubly skimmed with a total distance from nozzle to scattering center of 13.2 cm. The nozzle and skimmers are placed in a partitioned chamber that had two quadrant partitions for the nozzles and a scattering partition. These partitions are differentially pumped, allowing the protection of the ion detector from stray gas molecules, and hence false background signals.

The products from the collision are detected using a technique known as velocity map ion imaging. This technique involves resonance enhanced multi-photon ionization (REMPI) of the products with a laser and then accelerating the resulting ions perpendicular from the scattering plane using ion optics. They are then driven into a two-dimensional position-sensitive detector, consisting of microchannel plates, a phosphor screen and a charge-coupled device (CCD) camera. As products come in contact with the surface of the microchannel plate, a cascade of electrons is released. These electrons impact a phosphor screen, which converts the electron intensity into photons. These photons are then detected by the CCD camera, a device that collects the photons onto a two-dimensional array of capacitors, which accumulate a charge proportional to the

number of incident photons. This technique is known as velocity map ion imaging. [28] [29]

Figure 3 shows an example image taken using this setup. The colors represent the intensities of product molecules hitting the detector. [28] In the experiment shown, NO is detected after collision with Ar.

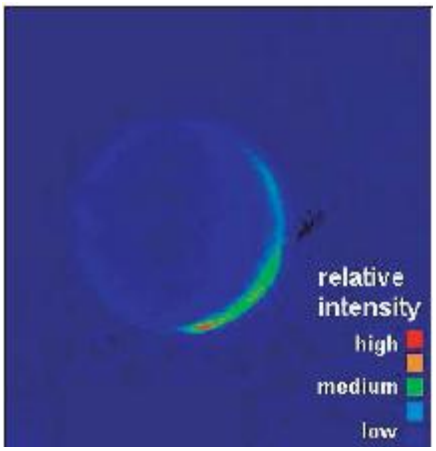


Figure 3. Product CCD camera image of cold molecules produced for the collision of NO with Ar. ©EDP Sciences, Società Italiana di Fisica, Springer-Verlag 2004. With permission of the European Physical Journal (EPJ). **[7]**

## I.E.3. Theory Behind Cooling Method

The bright spot in figure 3 depicts the cold molecules remaining after the "Billiard-like" scattering of two molecular beams. Elioff et al. have shown that this method can generate NO molecules with translational temperatures in the 300-500 mK range for the NO-Ar system via cooling due to collisional energy-transfer. They have shown that the zero-velocity condition is governed by two constraints that control the rebound velocity's magnitude and direction. The magnitude constraint is simplified to

$$\boldsymbol{v_{cm} = -u'_{NO}} \tag{1.3}$$

where the rebound velocity's magnitude is equal to the center-of-mass velocity. From this condition, an equation can be derived to define the product's internal energy in terms of the initial translational energy of NO and the ratio of the masses of the reactants.

$$\boldsymbol{E'_{rot}(NO_{v'=0,j'}) = \left(1 - \frac{m_{Ar}}{m_{NO}}\right) \times E_{trans}(NO_{v'=0,j=0.5})} \tag{1.4}$$

The direction of the rebound molecules can be derived from the Law of Cosines

$$\boldsymbol{v_{NO}^2 = v_{cm}^2 + u_{NO}^2 - 2u_{NO}v_{cm}\cos(\theta_{cm})} \tag{1.5}$$

so that $\boldsymbol{\theta_{cm}}$ is the angle between the center-of-mass velocity and the initial velocity of the NO molecules in the center-of-mass frame. Using definitions of the center-of-mass velocity and initial velocity of the NO molecules in the center-of-mass frame in terms of its laboratory frame velocity, the following equation is derived:

$$\boldsymbol{\cos(\theta_{cm}) = \frac{E_{Ar} - E_{NO}}{\sqrt{\left(E_{NO} + \left(\frac{m_{NO}}{m_{Ar}}\right)E_{Ar}\right)\left(E_{NO} + \left(\frac{m_{Ar}}{m_{NO}}\right)E_{Ar}\right)}}} \tag{1.6}$$

where the E's are the initial kinetic energies of NO and Ar. **[7]**

In the work proposed herein, we intend to create a crossed molecular beam setup similar to that used in the Chandler laboratory. It is our intention to seed each beam with the same molecule, and study the "self-collisions" of these species. When two molecules

with identical masses collide, both constraint equations simplify drastically. Equation 1.4 simplifies to

$$\boldsymbol{E'_{rot}(NO_{v'=0,j'})} = \left(\mathbf{1} - \frac{\boldsymbol{m_{NO}}}{\boldsymbol{m_{NO}}}\right) \times \boldsymbol{E_{trans}(NO_{v'=0,j=0.5})} = \mathbf{0} \tag{1.7}$$

and equation 1.6 simplifies to

$$\mathbf{cos}(\boldsymbol{\theta_{cm}}) = \frac{\boldsymbol{E_{NO} - E_{NO}}}{\sqrt{\left(\boldsymbol{E_{NO}} + \left(\frac{\boldsymbol{m_{NO}}}{\boldsymbol{m_{NO}}}\right)\boldsymbol{E_{NO}}\right)\left(\boldsymbol{E_{NO}} + \left(\frac{\boldsymbol{m_{NO}}}{\boldsymbol{m_{NO}}}\right)\boldsymbol{E_{NO}}\right)}} = \mathbf{0} \tag{1.8}$$

or $\boldsymbol{\theta_{cm}} = \mathbf{90}°$. Figure 4 shows a newton diagram that would be generated if two molecular beams, each composed of molecules with identical mass and velocity, collide at a 90 degree angle. A rebound angle of 90 degrees relative to the relative velocity axis would mean that the cold molecules would be found on the circle at the point where the collision first occurred. **[7]**

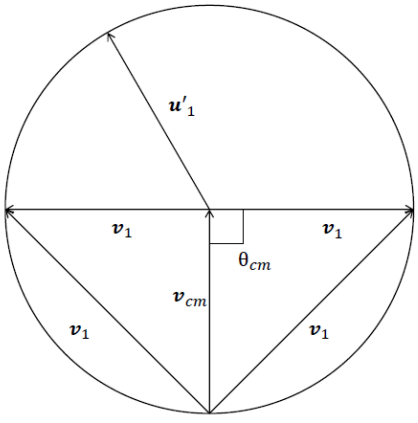


Figure 4. Newton diagram representative of self-collision

Elioff et al. were able to determine for the NO-Ar system that using their method, they could cool NO molecules in the rotational state J=7.5 to 406 mK. Later, using the same method, they were also able to measure the differential scattering cross-section with argon for this system for NO molecules in the J=1.5 to J=12.5 states. From this early work, they then expanded their method using atom-molecule collisions of equal mass. This was done using a $ND_3$-Ne system. For this system, the differential cross-section was also determined for this collision while monitoring $ND_3$ in the J=3 and J=2 states. The molecules in these states that were determined to be cold were found to have a translational temperature between 70 and 880 mK.

I.F. Duffy Lab Detection Method

The research being done by Dr. Duffy is in the field of molecular reaction dynamics, with an experimental emphasis on pure rotational spectroscopy. Molecular rotational motion, as with vibrational motion, is quantized. For example, the energy associated with these levels for a closed shell diatomic molecule is defined by equation 1.9.

$$\boldsymbol{E_J = J(J+1)\left(\frac{h^2}{8\pi^2 I}\right)} \tag{1.9}$$

In this equation, h is Planck's constant, I is the moment of inertia, and J=0, 1, 2,… is the rotational quantum number. These levels will not be equally populated, but will be distributed according to the Maxwell-Boltzmann distribution. Transitions between energy levels are governed by the specific selection rule $\Delta J=\pm 1$. It is an advantage of the

mm-wave technique that the gross selection rule for pure rotational spectroscopy is simply that the molecule has a permanent dipole moment. In other words, any polar molecule can be studied with this technique. [30]

Many molecules have rotational transitions spanning from the microwave region of the electromagnetic spectrum all the way into the terahertz and far infrared regions, depending on their molecular mass and degree of rotational excitation. While low frequency molecular bending modes of polyatomic molecules are excitable in the far-IR, in the mm-wave/sub mm-wave regions, only pure rotational transitions are accessible. It is this latter region from 50-330 GHz that the Duffy lab has access to.

If a molecule moves at non-relativistic speeds towards or away from a radiation source, it will experience a Doppler shift in frequency proportional to its velocity according to the relation,

$$\boldsymbol{\Delta\nu = \frac{v}{c}\nu_0} \tag{1.10}$$

where $\boldsymbol{v}$ is the velocity relative the source, c is the speed of light, and $\boldsymbol{\nu_0}$ is the rest transition frequency. If a molecule is moving towards a source, the crests of the wave pass the molecule in a shorter period experiencing a net increase in frequency and will therefore absorb radiation that was initially lower than its transition frequency. Likewise, an opposite shift will be found for motion in the opposite direction. [31] These shifts in the spectra and broadening of the lines can then be used to determine the molecular beam speeds and velocity spread of the parent and/or products.

The microwaves are detected using a cryogenically cooled hot electron bolometer, which works by detecting the thermal flux of absorbed radiation on an InSb surface that has been cooled to liquid helium temperatures. As electrons in the InSb crystal lattice absorb radiation, their mean temperature rises. This rise increases the mobility of the electrons, changing their resistance and hence the voltage across a biased resistor. **[32]**

The signal from the bolometer is then amplified twice. The first by a preamplifier connected directly to the bolometer and second by an amplifier with the ability to filter out unwanted noise. The amplified signal is then sent to an oscilloscope, which allows the measurement of the absorption of the mm-wave source frequency as a function of time. This oscilloscope is triggered by a signal sent from the pulse controller, which triggers the firing of a nozzle. To minimize random noise not already filtered as well as variations in the spectra, multiple individual triggering events are averaged. Afterwards, the final averaged spectrum is sent to a computer to be processed.

Normally, a scan does not consist of one single frequency but multiple frequencies within a selected span. The computer communicates to the microwave synthesizer to incrementally step until all of the frequencies within the span have been collected. By taking a span of frequencies around a transition, it allows the determination of the Doppler broadening and shifts. Once collected, the spectra are compiled into a single surface plot with time and frequency on the x-y plane and intensity along the z-axis as depicted in figure 8, which shows an example of a rotational line acquired in this manner, in this case the J=9←8 transition of OCS. When fit, the translational temperature spread along the mmWave probe axis yields a temperature of 100 K. Note,

since the lineshape evolves in time, transient changes in the Doppler profile may be observed with this technique.

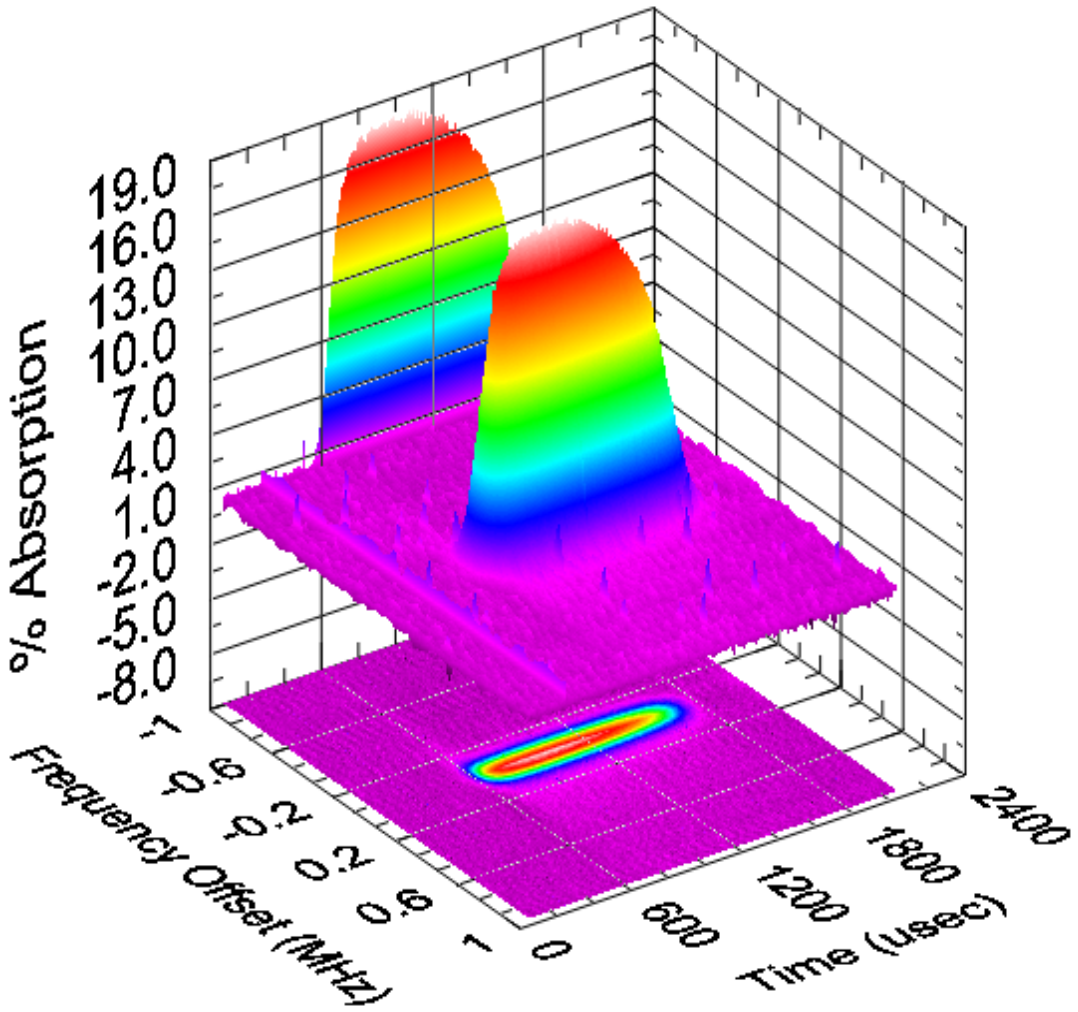


Figure 5. Surface plot of the J=9←8 (109463.0630 MHz) transition of OCS. The translational temperature of this line shape was determined to be approximately100 K.

# CHAPTER II

# EXPERIMENTAL

## II.A. Construction

The experiments described here require significant modifications to the molecular beam setup previously used in Dr. Duffy's research laboratory for photodissociation studies. These modifications, among others, included: a two arm machine, a chopper, custom circuitry pulse sequence for triggering, and a new gas inlet system. Both the two arm machine and the gas inlet system were constructed in conjunction with Nicholas Mark, whose work is in reactive radical scattering of chlorine and ozone. The chopper was constructed in conjunction with Josué Monge whose work is in Fourier transform Doppler spectroscopy.

### II.A.1. Two Arm Machine

The previous setup only employed one nozzle at a fixed angle, while research into crossed beam studies requires colliding two beams of gas. This is now remedied using a two arm machine that was designed to the desired specifications using Google Sketchup. The machine was designed so that the molecular beams would intersect the mm-Waves and each other in approximately the center of the chamber. For this to happen, each nozzle had to hang a total of 4 inches into the chamber from the lid.

To ensure free rotation, one arm was designed to be longer than the other so that the arms could connect at a central point while still allowing the nozzles to be at the same height. Figure 6 shows a picture of the completed arms. Each of the arms in the picture is hollow, allowing the nozzles to rest inside along with room for Teflon tubing to provide gas and BNC cables to provide triggering. Also included in the picture is the chopper, which is described in the next section.

The arms are attached to the lid through an aluminum collar, a Kwik-Flange™ six-way NW40 cross, and a threaded rod to hold the arms in place. The triggering for the nozzles are fed into the arms using Kwik-Flange™ BNC feed through flanges. The miniature diffusion pump is connected to the arms by a vacuum tube connected to the six-way cross.

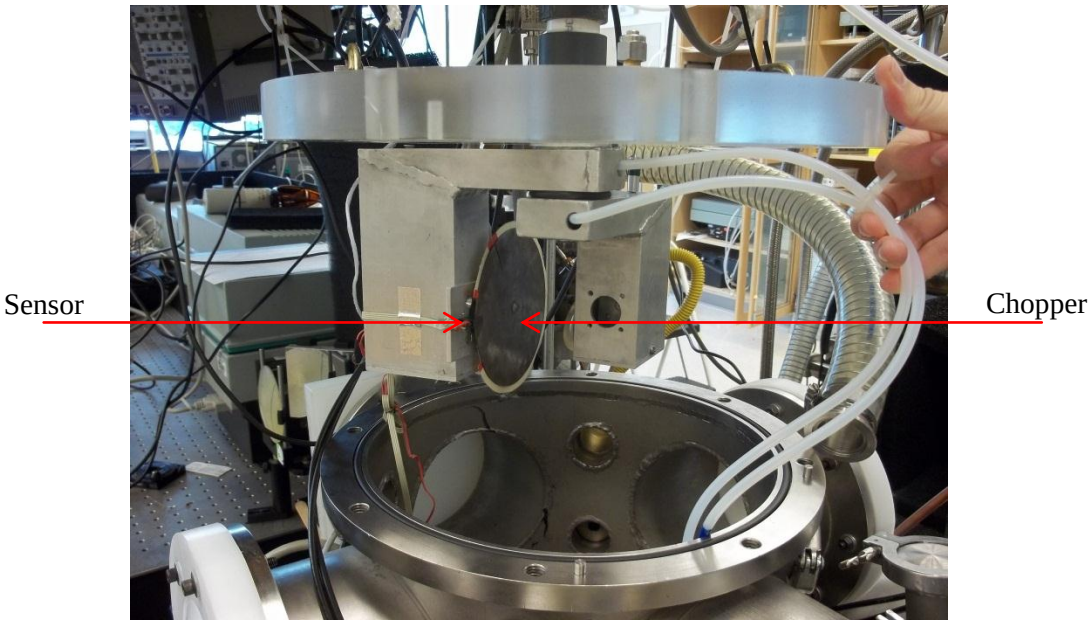


Figure 6. Picture of completed Two Arm Machine showing Teflon tubing and chopper with optical sensor.

### II.A.2. Chopper

The chopper is a stainless steel disk, which was fabricated by Bibey Machine Company in Greensboro. It was designed with a radius of 6 cm and a slit opening of 1.131 mm at the edge of the disk. The disc was fixed to a motor whose speed is dependent on the voltage applied to it. By doing this, the speed can be modified and hence the time the slit is open. The speed of the chopper was monitored using an Omron EE-SW1042 photomicrosensor. This sensor detects light transmitted from one side of its slot to the other. As the opening passes by, light makes it through, causing a signal. The chopper and sensor were attached to a bracket, which was screwed onto the slit nozzle's arm. Figure 6 shows the positioning of the chopper and sensor in relation to the arms. A paper disk was glued to the back of the chopper. The paper disk has a slit corresponding to the slit opening and a wider window opening that is used for chopper speed compensation in the pulse sequence circuitry as described in the next section.

### II.A.3. Pulse Sequence

The motor that was used in the creation of the chopper has been found to drift in speed. This drifting causes a mismatch in the nozzle timing. If the timing is off, very little to none of the gas from the pulse can make it through the chopper slit. To compensate for this, custom circuitry was created. This circuitry monitors the speed of the chopper, and changes the timing of the slit nozzle gas pulse to coincide the pulse with the opening on the chopper. To do this, it uses the "window" in the paper disk (see

Figure 7). As the chopper spins, light makes it through the window on the paper disk, causing a capacitor to charge. The voltage from the optical sensor is then used as the gate of a transistor which, when biased, charges this capacitor in constant current mode. Once the bias is removed the capacitor discharges. The subsequent circuitry triggers at a fixed voltage level on the negative slope. The faster the chopper turns, the earlier this trigger occurs firing the nozzle at the appropriate moment to coincide with the chopper slit opening.

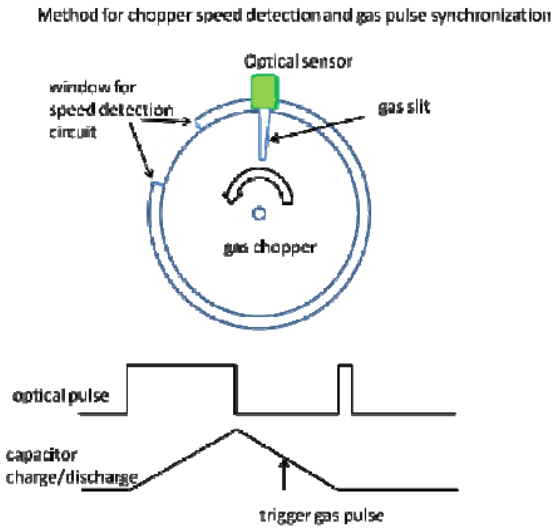


Figure 7. Schematic of Speed Detection Circuit. Capacitor charges as light makes it through detection window and discharges as it passes. The trailing edge of the resultant triangle wave is used to trigger slit gas pulse.

Using the trigger for the chopper slit opening created by the sensor circuitry, a pulse sequence circuit was created. This sequence allows three scans to be taken sequentially and repeatedly, compensating for pressure drifts that would normally occur between scans. Figure 8 shows the sequence. At 60 Hz, the chopper frequency is too fast to allow the valves to fire on every chopper cycle, as this would overwhelm the pumps.

To compensate for this, a chip was added to divide this trigger's frequency by 12. From this, three triggers are created, one for each nozzle firing independently and another for the collision, which are sent to separate oscilloscopes to trigger data collection. Based on these three triggers, two additional triggers are created consisting of the addition of one of the independent triggers with the collision. These triggers are sent to the Iota 1 pulse controller used to trigger gas pulses from the nozzle.

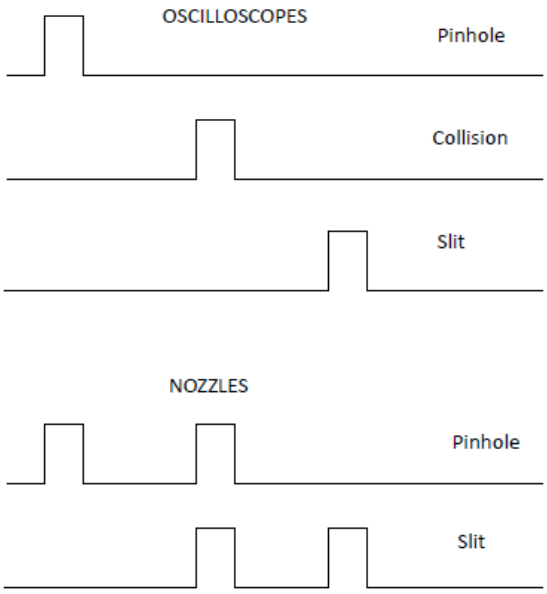


Figure 8. Pulse Sequence created. Top three triggers are sent to the oscilloscopes. Bottom two triggers are the addition of the upper (or lower) oscilloscope trigger and the center trigger. These are used to trigger the gas pulses.

### II.A.4. Gas Inlet System

The previous gas manifold system was not well suited to allow changing gas mixtures, monitoring the pressure of each nozzle independently, or switching the mixture that goes to each nozzle. A new gas inlet system was designed and built to be able to

accommodate each of these needs. The manifold was created using 1/4” stainless steel tubing with Swagelok connections. To monitor the pressure, two Baratron 1000 torr vacuum gauge transducers and one Baratron 10 torr vacuum gauge transducer was used. The 10 torr transducer was mainly used to check for leaks. To evacuate the system, a central line going to the pump system was added using 3/8” stainless steel with Swagelok connections. The entire inlet system was mounted above the reaction chamber in a vented cabinet, in case of leaks. Figure 9 shows the finished inlet system along with the original design.

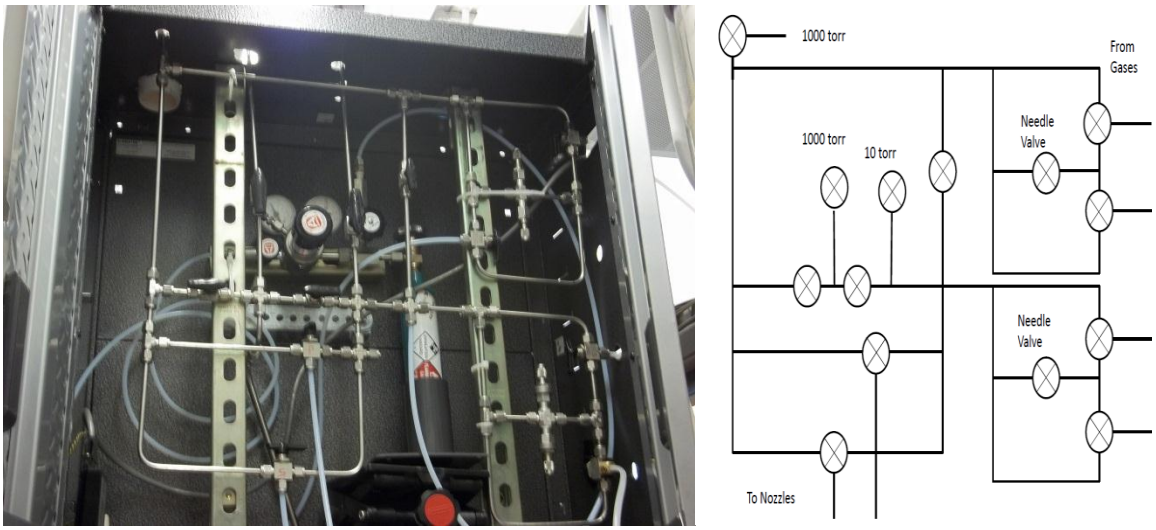


Figure 9. Completed Gas Inlet System inside vented cabinet and original design

## II.B. Programming

To accommodate the use of three scopes, the main LabVIEW program had to be modified. The first step in the modification was to create a command function to initialize each of the three Tektronix (model 2002) scopes with the settings that would be

used for that particular scan. This was done with a slight modification of the code already in place. The code was designed to use a LeCroy 9370 oscilloscope. Each command provided by LeCroy for use with LabVIEW has an analogous function provided by Tektronix. By swapping the commands and duplicating twice, it allowed an easy transition from the LeCroy to Tektronix scopes. The second modification required deconstructing the time array used for the LeCroy scope and reformatting it to work for the Tektronix scopes. The third modification required modifying the output command previously used to communicate with the new scopes and retrieve the necessary data. Along with this modification, a program delay had to be added in to account for the communication speed difference between the scopes. The final modification was to allow the user to choose between collection methods. By doing this, it allows using the scopes in a manner that is necessary for the experiment and not based on what the program dictates.

Another program was created to write a database for cataloging and searching past scans. With the volume of data collected in the lab, it can be tedious to find other scans that use a given molecule, setup, or other parameters. Data fields include gas inlet conditions such as stagnation pressure, mixture ratios, parent molecule/molecules, parent pressures, and gas pulse widths. Data fields corresponding to laser use consist of laser polarity, source, wavelength, laser power, laser energy, laser spot size, and laser repetition rate. Data fields for beam geometry include beam angles (relative to the mmWave axis) and experimental geometry image setup. Data fields for amplifier settings include gains,

couplings, and frequency rolloffs. Data fields for the mmWaves include power, polarization, target voltage, detector bias, and detector gain.

## II.C. Description of Apparatus

### II.C.1. Reaction Chamber

For this experiment, the apparatus consisted of three main parts: the reaction chamber, the mm-Waves, and the detector. A schematic of the reaction chamber is shown in figure 10. The reaction chamber was pumped using a three pump system. The first pump was an Edwards XDS 10 scroll pump with a pump speed of 15 L/min. The second pump was an Edwards mechanical booster pump model EH-250 with a pump speed of 3992 L/min. The final pump was a Varian VHS-6 diffusion pump with a pump speed 2400 L/s. With this system, the average pressure within the chamber before gas was added was $5x10^{-6}$ torr. The pressure throughout the system was monitored by 3 Edwards ACT-E gauges and a Varian 0571-K2471-304 ionization gauge.

As mentioned earlier, hanging down from the top of the chamber were to differentially pumped "arms", housing the nozzles. Each of these arms was free to rotate completely around the chamber. Based on the previous experiments by David Chandler **[7] [25]**, the arms were set at a 90 degree angle from each other and 45 degrees from the mm-Wave axis. A nozzle was situated inside each arm along with the necessary tubing and wiring. These arms in turn were pumped using a Leybold Heraeus miniature diffusion pump with a speed of 75 L/s. The average pressure within the arms before gas was introduced was below $2x10^{-2}$ torr, the lower limit of the pressure sensor.

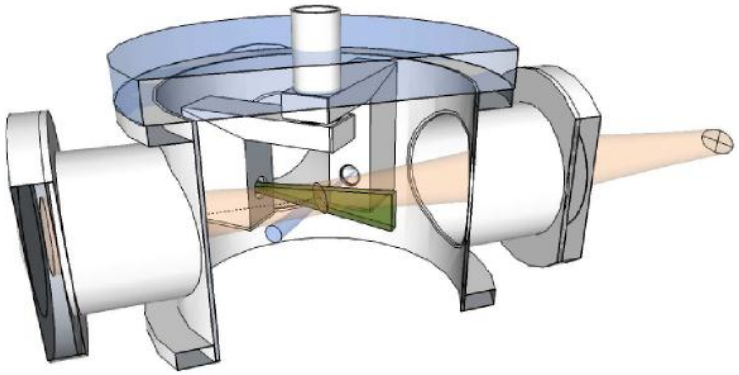

Figure 10. Cross Section of reaction chamber including two differentially pumped “arms”, each housing a pulsed nozzle. The molecular beams and mmWave beam are depicted in blue/green and red, respectively.

II.C.2. mm-Waves

The mm-Waves used in this experiment were produced using an HP 83623B series swept signal generator, which can produce frequencies from 10 MHz to 20 GHz with a 1Hz frequency resolution. This synthesizer was connected to either an Agilent Technologies 83557A or 83558A source module, which increases the range of the synthesizer up to either 50-75 GHz or 75-110 GHz, respectively. Depending on the frequency required, either a doubler (Millitech MUD-06-LF000 (50-75GHz) or Virginia Diodes VDI-WR5.1x2 (75-110GHz)) or tripler (Virginia Diodes VDI-WR3.4x3 (75-110GHz)) can be used coupled with a Spacek Labs power amplifier. These allow the range of frequencies to extend up to 330 GHz.

The mm-Waves were focused into the scattering region of the chamber by 2 lenses. The first lens was plano convex and made of polymethylpentene, commonly known as TPX, with a focal length of 15.2 cm. The second lens was biconvex and made

of high density polyethylene (HDPE) with a focal length of 26.9 cm. This lens is also used as a flange for one of the chamber ports. After interaction, the mm-Waves were focused toward the detector by two more lenses. The first was another biconvex lens flange with twice the focal length of the other. The second was made of TPX and was used to focus the mm-Waves into the detector window.

### II.C.3. Detector

The mm-Waves were detected using a QMC InSb hot electron bolometer model QFI/X. This bolometer was housed in a closed cycle cryostat built by ColdEdge Technologies. The bolometer was cooled below 4 K by an SDRK-408 cryocooler from Sumitomo. A schematic of the detector apparatus is shown in figure 11. The two stage cryocooler cold head is suspended from a stand into a vacuum insulated dewar. An open area between the cold head and the dewar is filled with gaseous helium to serve as a vibration free thermal transfer medium between the cold head and the detector. The pressure inside this region stays below 0.30 psi.

The cryocooler has two stages: a 30 K stage and a 4 K stage. As compressed helium is pumped through the cold head, the temperature inside the head slowly drops. When the head reaches 30 K, the second stage opens, rapidly cooling the temperature down to 4 K.

As the cold head is cooling, gaseous helium in the vibration free region carries heat away from the cold head to the vacuum jacket, cooling itself. When the temperature of the vibration free region reaches 4 K, the gaseous helium condenses on the baseplate.

Liquid helium will continue to accumulate as long as long as the cold head is on. This allows the temperature of the baseplate to stay constant for a short time after the cold head has been turned off.

The bolometer chip is directly connected to the baseplate using a copper mount. The mounting system allows heat from the bolometer to be pulled away through the baseplate into the vibration free region, keeping the bolometer cold. Next to the bolometer is a Winston cone, which has 3 main roles: directs and concentrates the mm-Waves from the window onto the bolometer, restricts the radiation the bolometer experiences to only what comes out of the cone, and ensures an even distribution of the radiation on the bolometer. [33]

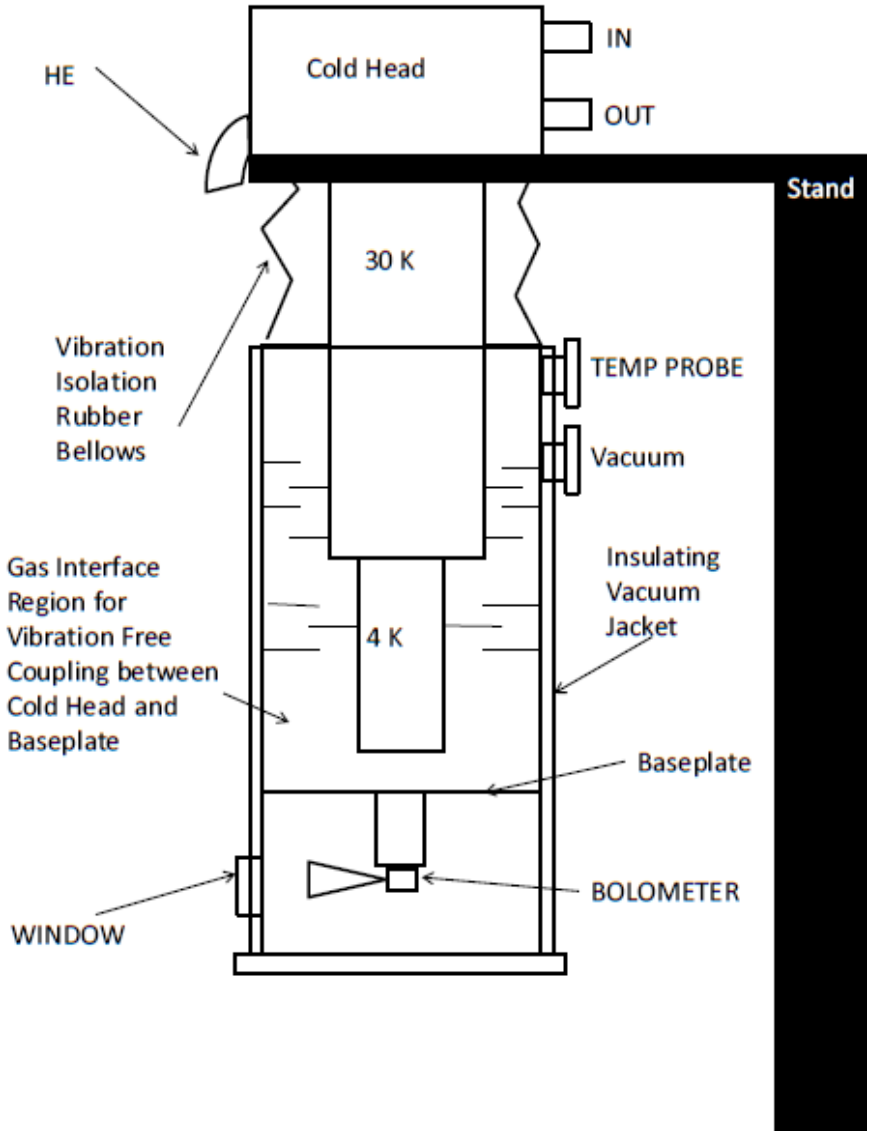


Figure 11. Schematic of the detector including fins, cryocooler, and bolometer

## II.D. Settings for $N_2O$-$N_2O$ Experiment

For this experiment, the nozzles were controlled using a Parker Hannifin Iota One pulse controller. Each nozzle was triggered independently using the pulse sequence

described earlier. The slit nozzle was set to a 650 μs on time, while the pinhole was set to a 500 μs on time. The delays for both nozzles were set to zero.

The slit nozzle was found to work best at pressures between 700 and 800 torr, so it was kept at 750 torr. This nozzle was skimmed using a razorblade skimmer to eliminate spread perpendicular to the beam plane. To minimize clustering that can often occur in the slit nozzle, $N_2O$ was seeded with Ar in a 50/50 mixture. Even with dilution, the slit is suspected of cluster in the center of the beam, causing a bilobal divergence in the beam perpendicular to the nozzle slit axis. To eliminate the effects of this divergence, a wedge was added so that only one of these lobes would make it through the skimmer and into the reaction chamber. The pinhole, on the other hand, does not cluster as readily as the slit nozzle, so pure $N_2O$ was used. In order to maximize the amount of atoms reaching the reaction space, pressure for this nozzle was kept constant at 1000 torr. Both nozzles were monitored using individual 1000 torr Baratron pressure transducers.

The signals produced from the detector first passed through a QMC model ULN95 low noise preamplifier set for x100 gain. It was then passed to a Stanford Research Systems SR560 Low Noise Preamplifier with a high pass filter of 30 Hz. This signal was sent to the three Tektronix TDS 2002 oscilloscopes triggered individually using the pulse sequence mentioned earlier. These oscilloscopes were set to single acquisition mode and the signal was averaged over 64 sweeps.

After averaging, the signals were sent using GPIB cables to a computer running LabVIEW. Using a program previously written, the frequency span, increment, and center frequency were chosen. Figure 12 shows the front panel of the main program and

the front panel of the frequency selection program. The theoretical transition frequencies were downloaded from NASA's Jet Propulsion Lab spectroscopy database. [34]

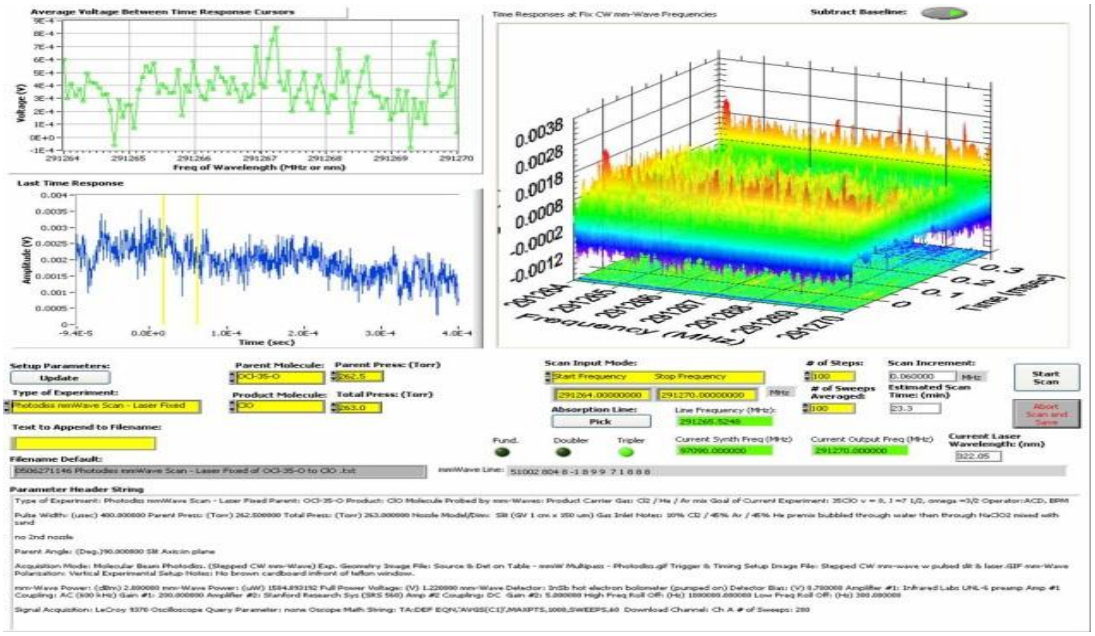


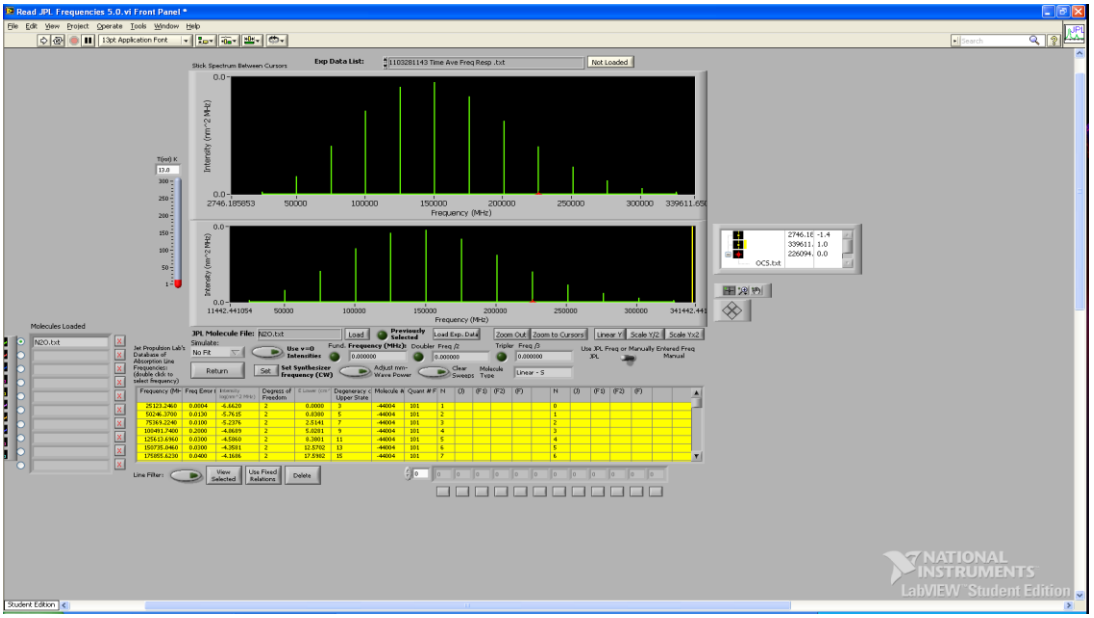


Figure 12. Front Panels of LabVIEW Main Program and Frequency Selection Program

## III.E. Experimental Difficulties

Research involving instrument development necessarily involves unforeseeable complications. Shortly after work on this project first started in the Duffy lab, the liquid helium detector was sent away to be turned into a closed cycle system. The original estimate for delivery was quoted as 12 weeks. This period turned into 12 months for various reasons. With no detector, our research focused on construction of the new crossed beam setup. When the detector arrived, it was determined that the window on the dewar and the Winston cone were misaligned. To fix this, copper shims were added to make the Winston cone lineup with the detector window. Indium foil was also added between the shims and the mounting block to increase thermal conductivity. The bolometer chip's operation was found to be intermittent and after a month, the chip stopped functioning. A replacement was sent approximately one month after our request for a new one.

One of the components of the closed cycle system was a Sumitomo F-70L helium compressor. The lines running from this compressor are braided steel and are meant to be insulated to prevent loss of helium. One of these lines mysteriously sprung a leak, releasing all of the helium stored in the compressor slowly into the lab. This line had to be replaced and the compressor recharged with helium. The compressor also requires a significant flow of cold water to keep its compressor cool. This requirement was met by connecting the compressor to the building "chilled" water lines. Unknown at the time,

the “chilled” water system does not work when the temperature outside is below 35°F, limiting the times during the year that the detector could be used.

Another issue that occurred was an overheating of the 220V plug leading to the diffusion pumps. The plug being used was not rated to handle the 12 A of current being fed into the diffusion pump and eventually, the plug melted. This plug had to be replaced using a medical grade plug to handle the heat generated.

Most recently, the power amplifier that connects to both the doubler and tripler on the source modules was connected incorrectly, causing a reversed bias on the amplifier. This was sent back to the manufacturer and has yet to return. Without this amplifier, the frequencies available are greatly diminished.

# CHAPTER III

# RESULTS AND DISCUSSION

## III.A. Data

The results here are preliminary as the majority of the time spent on this work was used in construction of the apparatus. The data for this experiment was taken in two parts. First, a background was taken for each scan with the nozzles firing. During this scan, gas was not opened to the nozzles so no signal from reactant gas molecules should be seen. All other settings were held constant. Second, gas was allowed to the nozzles and a second set of scans were taken. After scans were taken, the background scans were subtracted from the gas containing scans to remove any artifacts that are a result of background noise (e.g. spikes, random radiation, etc.). Scans of the J=6←5 transition for the self-collision of $N_2O$ are shown in figure 13. In these scans, the frequency span was 1 MHz over a total of 50 steps.

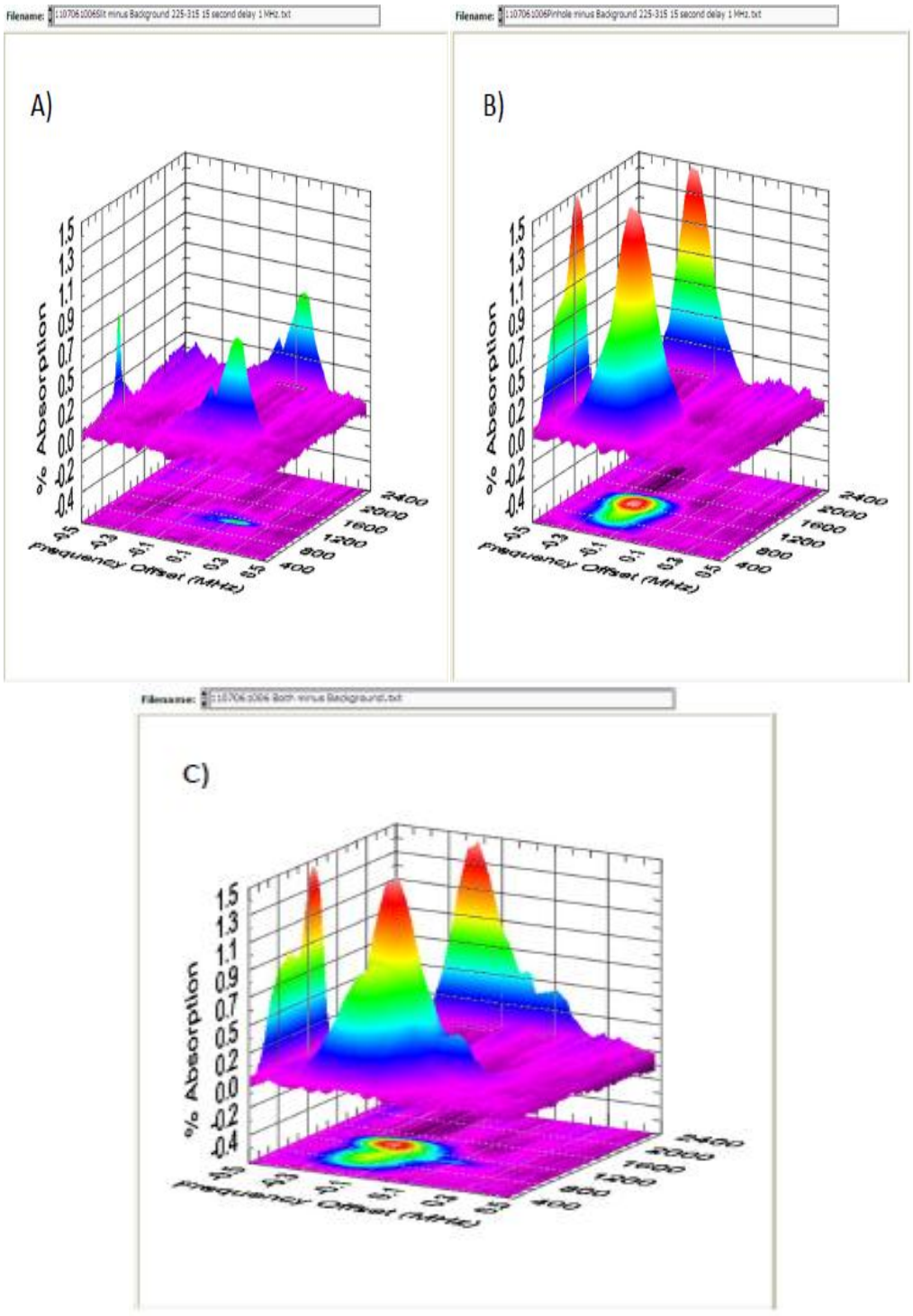


Figure 13. Scans of the J=6←5 (150735.046 MHz) transition of $N_2O$. A) Individual Slit nozzle minus Background. B) Individual Pinhole nozzle minus Background. C) Both nozzles firing minus Background

The Doppler shift due to the arm angles can clearly be seen as both individual peaks are approximately shifted by +/- 0.2 MHz on either side of the center frequency. Also shown in these scans is the fact that adding the individual scans together would not be the same as the scan of both nozzles firing simultaneously (i.e. collision scan). From this, we can conclude that a collision occurred. By subtracting the individual scans from the collision scan, the resulting positive peaks should be post collision products. Figure 14 shows the result of this subtraction.

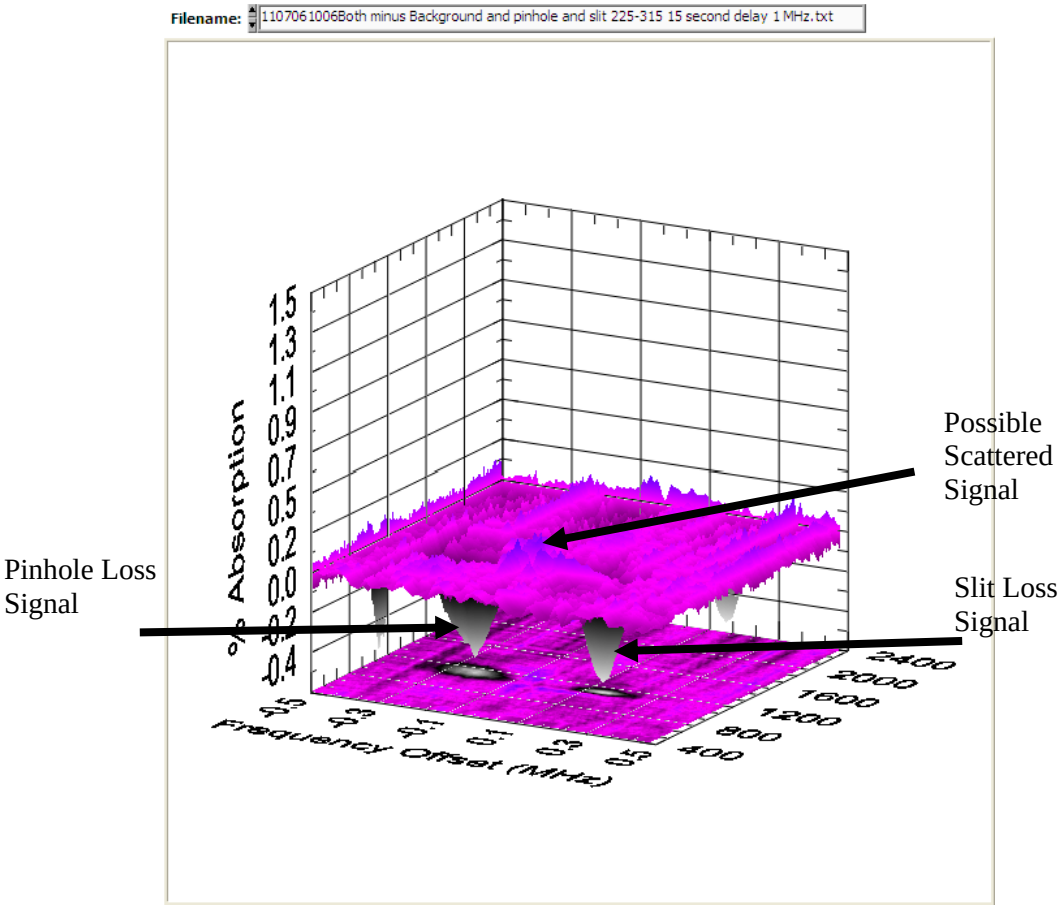


Figure 14. Surface plot resulting from the subtraction of the individual scans from the collision scan

There is still a small broad positive peak, possibly indicative of post collision products. However, these products are too wide in frequency to be considered cold. If cold molecules had been created, the resultant peak would be narrow in frequency due to minimal motion in the laboratory frame.

There could be multiple reasons for the absence of cold molecules. First, they could have been swept away by collision with molecules entering the scattering region after their creation. In this case, either pressure or nozzle timing could be modified so the last molecules entering the scattering region have the requisite conditions for creating cold molecules.

For the preliminary diagnostic work on this experiment, $N_2O$ was chosen for its low cost and low toxicity. It is only weakly polar resulting in weaker transition lines. This weakness could result in signals from cold molecules too small to be separated from the background. Substituting a molecule such as DCl or OCS that has a strong dipole moment would ensure a strong signal from any cold molecules produced.

The frequency increments used in averaging the data in figure 14 were too large to see the cold molecules. The 0.5 MHz span and 0.1 MHz step size used in these scans could have stepped right over the frequency of cold molecules, which is expected to be only 10-20 kHz wide, precluding the possibility of accurately confirming their production. While finer scans were taken, no signals for cold molecules above background noise levels were observed. Shortly after taking this preliminary data, we discovered the averaging feature of the Tektronix scopes we were using did not store more than 8-bits of voltage data at a given time point. This means that this particular

model of oscilloscope throws away the low signal level data we need to accumulate. Following this realization, we undertook a new data acquisition method that involved averaging on the computer. We have not had time to test this on our scattering experiments.

III.B. Fitting and Collisional Cross-Section Determination

Even though cold molecules were not produced, the collisional cross-section for the self-collision of $N_2O$ was still determined. To do this, the line shapes were fit using a Voigt profile to determine the number density and relative velocity of each beam. A Voigt profile is a line profile that is the result of the convolution of a Gaussian profile, G(x), and a Lorentzian profile, L(x). Equation 3.1 is the equation for this convolution. [35]

$$\boldsymbol{G(x) * L(x) = \frac{1}{\sqrt{2\pi}} \int_{-\infty}^{\infty} G(y) L(x-y) dy} \tag{3.1}$$

The Gaussian portion arises from Doppler broadening within the beam due to large velocity distributions. In the case of the cold molecules, this should be very minimal due to a very narrow velocity distribution. The Lorentzian portion comes largely from a combination of residual pressure broadening as well as transit time broadening.

The Voigt profile, as presented by Armstrong can be found in equations 3.2-3.6 [36]:

$$\boldsymbol{P(x,y) = \frac{1}{\alpha_D}\left(\frac{\ln 2}{\pi}\right)^{1/2} K(x,y)} \quad (3.2)$$

$$\boldsymbol{K(x,y) = \frac{y}{\pi}\int_{-\infty}^{+\infty} \frac{e^{-t^2}}{y^2+(x-t)^2}\,dt} \quad (3.3)$$

where

$$\boldsymbol{y = \frac{\alpha_L}{\alpha_D}(\ln 2)^{1/2}} \quad (3.4)$$

$$x = \frac{v-v_0}{\alpha_D}(\ln 2)^{1/2} \quad (3.5)$$

$$\alpha_D = v_0\left(\frac{2kT\ln 2)}{Mc^2}\right)^{1/2} \quad (3.6)$$

In these equations, $\alpha_D$ and $\alpha_L$ correspond to the Doppler and Lorentzian half-widths at half max, respectively, and $v_0$ is the theoretical transition frequency.

The fits generated with these equations for the individual pinhole and slit nozzle scans are shown in figures 15 and 16, respectively. In these figures, the top graph corresponds to the absorbance measured as a function of frequency. The times used for these absorbances are shown by the yellow cursors in the bottom portion. The bottom graph corresponds to an overlay of each of the averaged absorbance vs. time traces from the oscilloscope.


Figure 15. Fit generated for the pinhole individual scan. A) Absorbance as a function of frequency with the transition line in green. B) Overlay of each averaged absorbance vs. time trace received from the oscilloscope

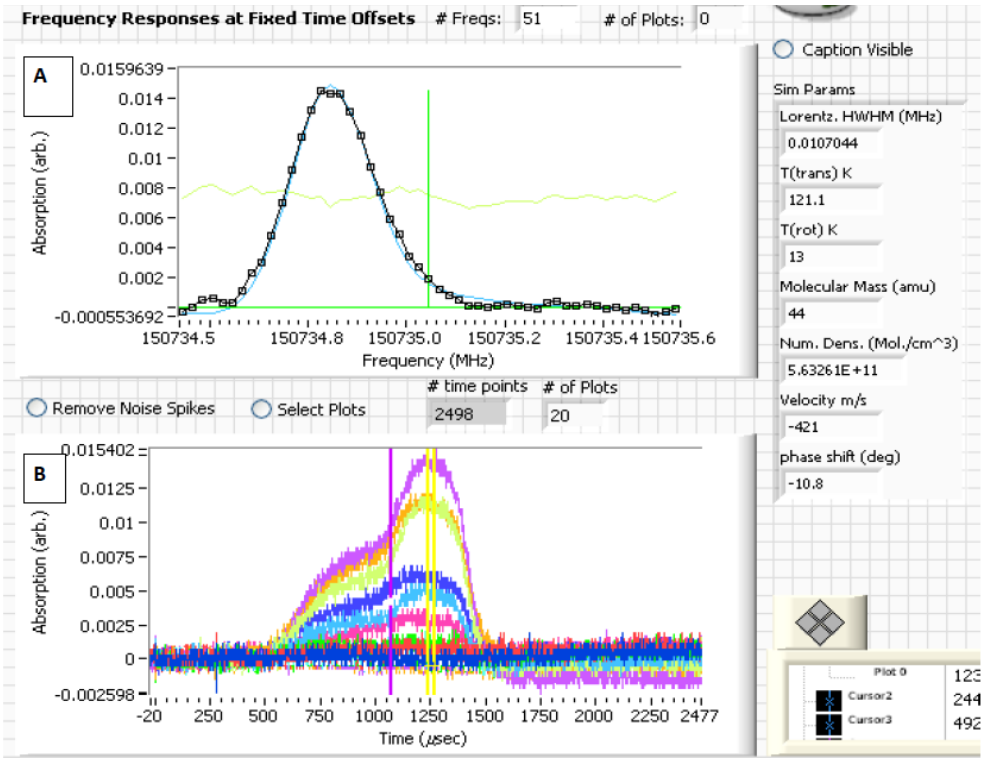


Figure 16. Fit generated for the slit individual scan. A) Absorbance as a function of frequency with the transition line in green. B) Overlay of each averaged absorbance vs. time trace received from the oscilloscope

On the right side of these figures, the parameters used to produce the fits are shown. The velocity fitting parameter refers to the velocity of the molecules relative to the mm-Wave axis, with negative velocities indicating movement toward the source, and vice versa. Using these velocities, the transition frequency, and equation 1.10, the Doppler shift for the pinhole and slit were determined to be -0.211 MHz and 0.161 MHz, respectively.

The number densities produced from these fits can change based on the rotational temperatures within the beam. Table 1 shows the fits for both the pinhole and slit nozzles

as a function of rotational temperature determined with all of the same parameters given in the original fits.

Table 1. Relating $T_{rot}$ to number density for the slit and pinhole nozzle (same parameters as previous fits).

| $T_{rot}$ | Slit | Pinhole |
|---|---|---|
| 10K | $2.0 \times 10^{13}$ cm$^{-3}$ | $5.5 \times 10^{13}$ cm$^{-3}$ |
| 20K | $2.8 \times 10^{13}$ cm$^{-3}$ | $7.6 \times 10^{13}$ cm$^{-3}$ |
| 30K | $4.4 \times 10^{13}$ cm$^{-3}$ | $1.2 \times 10^{14}$ cm$^{-3}$ |
| 40K | $6.3 \times 10^{13}$ cm$^{-3}$ | $1.8 \times 10^{14}$ cm$^{-3}$ |

The actual rotational temperatures of the molecules in the beams were never measured for $N_2O$. In the past, the lab has used OCS as a molecule of interest and for this molecule the rotational temperature has been determined to be around 30K. Since $N_2O$ is smaller with fewer rotational lines than OCS, it is easier to cool rotationally, so an estimated rotational temperature of 20 K would be reasonable. In our estimate of the $N_2O$ scattering cross section below, we will use this rotational temperature and the densities this implies.

For this collision, there are two separate energy pathways that could occur. The first pathway involves changing rotational state as shown in equation 3.7.

$$\boldsymbol{N_2O(v";J" = 5) + X \rightarrow\ N_2O(v';J') + X} \tag{3.7}$$

where X=$N_2O$ or Ar. The cross section for collisions occurring in this pathway is defined as

$$\sigma_{J"_{Total}} = \sum \sigma_{J"-J'} \tag{3.8}$$

The second pathway is a velocity changing pathway shown in equation 3.9.

$$N_2O(v";J" = 5) + X \rightarrow N_2O(v';J' = 5) + X \tag{3.9}$$

While inelastic velocity changing collision cross sections can be large, most of these do not change the final direction of the scattered molecule enough to be observed with our setup. Our technique, however, can monitor the first pathway, with our loss signal corresponding to the molecules scattered out of the J=5 rotational state. We assume that collisions that move population into J=5 do not contribute to the parent or loss signals since these would be Doppler broadened significantly. Therefore, cross sections determined in this work mostly corresponds to the first pathway.

Based on the number density parameters obtained, a total rotational state changing collision cross-section was determined using equation 3.11 [37]:

$$\boldsymbol{\sigma_{AB}} = \frac{\boldsymbol{\rho_{scat}}}{\boldsymbol{\tau_{interact}\langle u_r\rangle \rho_A \rho_B}} \tag{3.11}$$

where $\rho_{scat}/\tau_{interact}$ is the collision frequency per unit volume, $\rho_A$ and $\rho_B$ are the number densities of reactants A and B, and $\langle \boldsymbol{\mu_r} \rangle$ is the average relative velocities of the reactant molecules. If we assume that every collision leads to scattered molecules, $\rho_{scat}/\tau_{interact}$ is also equal to the number of scattered molecules formed per unit volume per unit time.

Using the velocity relative to the mm-Waves, the actual beam velocities were determined as 595.4 m/s and 454.0 m/s for the pinhole and slit nozzles, respectively. Based on these velocities, the average relative velocity was determined to be 748.7 m/s.

Using this velocity and the number densities in table 1, table 2 shows the parameters determined for the 20 K rotational temperature using equations 3.12-3.16. [38]

$$\frac{I}{I_0} = e^{-\alpha_{max}L} \tag{3.12}$$

$$\%Abs = \left(1 - \frac{I}{I_0}\right) * 100 = (1 - e^{-\alpha_{max}*L}) * 100 \tag{3.13}$$

In these equations, $\alpha_{max}$ is the absorption coefficient at the transition frequency in $cm^{-1}$, L is the path length, which is assumed to be 1.25 cm for these calculations, and $I_0$ and I correspond to the intensity of the mmWaves before and after interaction, respectively. Solving for $\alpha_{max}$ yields

$$\alpha_{max} = \frac{-\ln\left(1-\frac{\%Abs}{100}\right)}{L} \tag{3.14}$$

This can then be substituted into equation 3.15, where $I_{AB}(T)$is defined by equation 3.16 and $\Phi_{AB}$ corresponds to the amplitude of the area normalized Voigt profile at line center.

$$\rho_{scat} = \frac{\alpha_{max}}{I_{AB}(T)*\Phi_{AB}(\nu_0)} \tag{3.15}$$

$$I_{AB}(T) = \frac{8\pi^3}{3hc}\nu_0 S_{BA}{\mu_x}^2 \frac{e^{\frac{-E''}{k_bT}} - e^{\frac{-E'}{k_bT}}}{Q_{rs}(T)} \tag{3.16}$$

In these equations, $I_{AB}(T)$ corresponds to the line intensity in $cm^2$ per second for the temperature in question and determined from cataloged intensities on JPL's website. [34] E' and E'' are the energies of the upper and lower states in $cm^{-1}$, respectively. $S_{BA}$ is the

line strength, $\mu_x$ is the dipole moment in Debye, $\nu_0$ is the frequency of the transition in MHz, and $Q_{rs}(T)$ is the rotation-spin partition function determined using the energies and degeneracies provided by JPL. It describes how the molecules are partitioned over the rotational energy levels as a function of temperature.

Based on the definition of the collision frequency given earlier, $Z_{AB}$ can be defined by equation 3.17. The time variable is the time from first product formed to last product formed. In this work, this was calculated as the time the chopper slit is open as roughly 50 μs. This represents the upper limit of the interaction time. Based on this, the cross-sections obtained are the lower limit of the actual cross-section.

$$\frac{Z_{AB}}{\Delta V} = \frac{\rho_{scat}}{\tau_{interact}} \tag{3.17}$$

By substituting equations 3.14, 3.15, and 3.17 into equation 3.11, the equation for the cross-section in terms of the percent absorption of scattered molecules and the initial number densities is given by

$$\sigma_{AB} = \frac{\rho_{scat}}{\tau_{interact}\langle u_r\rangle\rho_A\rho_B} = \frac{-ln\left(1-\frac{\%Abs}{100}\right)}{L*\tau_{interact}*\langle u_r\rangle*\rho_A*\rho_B*I_{AB}(T)*\Phi_{AB}(\nu_0)} \tag{3.18}$$

Since the positive peak in figure 14 is too small to fit, the negative peak from subtraction of the pinhole "loss" signal was used. The percent absorption of this peak was used in the calculation of the product number density.

Table 2. Results of the rotational state changing cross-section determination. $\sigma_{AB}$ is the cross-section for the J=5 rotational level scattering from a molecular beam with a 20K rotational temperature distribution

| | |
|---|---|
| $Q_{rs}(20\ K)$ | 33.5113 |
| $\boldsymbol{I_{AB}(20\ K)}$ | $3.57\text{x}10^{-11}$ $cm^2s^{-1}$ |
| $\boldsymbol{\rho_{scat}}$ | $1.5\text{x}10^{13}$ $cm^{-3}$ |
| $\boldsymbol{Z_{AB}}$ | $3.0\text{x}10^{17}$ $cm^{-3}s^{-1}$ |
| $\boldsymbol{\sigma_{AB}}$ | 9 $Å^2$ |

Note: Densities and Collision Frequencies based on fit of rotational line shapes and assume $T_{rot}$=20 K

During the calculation of these cross-sections, some assumptions had to be made. The first assumption was that both molecular beams have the same rotational temperature. These temperatures were never measured, so the cross-sections calculated are only a rough estimate. Second, an assumption is made that mmWave beam width is not larger than the interaction volume. If the width is larger than the interaction volume, the actual number densities would be higher than those calculated, meaning the densities calculated are a lower limit of the actual densities.

## III.C. Conclusion

A crossed molecular beam instrument was constructed to allow new crossed beam methods to be employed in the Duffy lab. This included new differentially pumped "arms" and a gas inlet system to replace the manifold already in use. A chopper was constructed to shorten the gas pulses emanating from the slit nozzle, allowing the production of cold molecules to be possible using Chandler's "Billiard-like" scattering method. A custom pulse sequence circuit was also constructed to allow the production of

three scans in a given run, reducing the systematic error associated with the stagnation pressure drift. This pulse sequence was also used to monitor and adjust the nozzle timing based on drifts in the chopper speed to ensure gas made it through the chopper opening.

Unfortunately, cold molecules were never observed during this work. There are many possible reasons for this including: cold molecules were swept away after creation by other molecules entering the scattering region, a more polar molecule is required, and the signal levels were too low for the resolution of the employed oscilloscopes. In the future, these issues can be remedied and cold molecules may be produced using this method.

As mentioned earlier, a problem in the acquisition method was remedied shortly after completion of this work. The Tektronix scopes only stores 8-bits of data during the averaging, whereas the LeCroy scope stores 16-bits. The new method involves collecting each individual time trace on the LeCroy scope and sending it to the computer for averaging. The computer is told how many traces to average, raising the limit of averages from 60 to almost 10,000. Using a trigger rate of 60 Hz, in the same time it took to take 60 traces, the system can now average 1000.

The total rotational state changing cross-section was calculated for the self-collision of $N_2O$. This cross-section was calculated, assuming a rotational temperature of 20 K for fitting the rotational line shape. While not quantitative, the cross-section determined for the self-collision of $N_2O$ is reasonable for this preliminary test of the instrument.

BIBLIOGRAPHY

[1] W. Greiner and B. Muller, Guage Theory of Weak Interactions, Berlin: Springer Verlag, 2000.

[2] H. L. Bethlem and G. Meijer, "Production and application of translationally cold molecules," International Reviews in Physical Chemistry, vol. 22, no. 1, pp. 73-128, 2003.

[3] C. C. Bradley, C. A. Sackett, J. J. Tollett and R. G. Hulet, "Evidence of Bose-Einstein Condensation in an Atomic Gas with Attractive Interactions," Phys. Rev. Lett., vol. 75, no. 9, pp. 1687-1690, 1995.

[4] R. V. Krems, "Molecules near absolute zero and external field control of atomic and molecular dynamics," International Reviews in Physical Chemistry, vol. 24, no. 1, pp. 99-118, 2005.

[5] M. Schnell and G. Meijer, "Cold Molecules: Preparation, Applications, and," Angew. Chem. Int. Ed., vol. 48, pp. 6010-6031, 2009.

[6] D. W. Chandler and K. E. Strecker, "The Quest fot Cold and Ultracold Molecules," ChemPhysChem, vol. 10, pp. 751-754, 2009.

[7] M. Elioff, J. Valentini and D. Chandler, "Formation of NO(j'=7.5) molecules with sub-kelvin translational energy via molecular beam collisions with argon using the technique of molecular colling by inelastic collisional energy-transfer," Eur. Phys. J. D, vol. 31, pp. 385-393, 2004.

[8] A. Einstein, "Über einen die Erzeugung und Verwandlung des Lichtes betreffenden heuristischen Gesichtspunkt," Annalen der Physik, vol. 17, no. 6, pp. 132-148, 1905.

[9] R. A. Millikan, "The electron and the light-quanta from the experimental point of view" Nobel Lecture, Stockholm, 1924.

[10] L.-V. de Broglie, On the Theory of Quanta, University of Paris, 1924.

[11] R. S. Berry, S. A. Rice and J. Ross, Physical Chemistry, New York: John Wiley and Sons, 1980.

[12] R. Frisch, "Experimental Demonstration of Einstein's Radiation Recoil," Zeitschrift fuer Physik, vol. 86, pp. 42-48, 1933.

[13] J. L. Picque and J. L. Vialle, "Atomic-beam deflection and broadening by recoil due to photon absorption or emisiion," Optics Communications, vol. 5, pp. 402-406, 1972.

[14] T. W. Hansch and A. L. Shawlow, "Cooling of Gases by Laser Radiation," Optics Communications, vol. 13, no. 1, pp. 68-69, 1975.

[15] Wineland and Dehmelt, *Bulletins of the American Physical Society.*

[16] D. H. Wineland, H. E. Drullinger and F. L. Walls, "Radiation-Pressure Cooling of Bound Resonant Absorbers," Physical Review Letters, vol. 40, no. 25, pp. 1639-1642, 1978.

[17] W. D. Phillips, "Laser cooling and trapping of neutral atoms," Reviews of Modern Physics, vol. 70, no. 3, pp. 721-741, 1998.

[18] W. T. Luh, K. M. Sando, A. M. Lyyra and W. C. Stwalley, "Free-bound-free resonance fluorescence in the K2 yellow diffuse band: Theory and Experiment," *Chemical Physics Letters,* vol. 144, pp. 221-225, 1988.

[19] W. T. Luh, J. T. Bahns, A. M. Lyyra, K. M. Sando, P. D. Kleiber and W. C. Stwalley, "Direct excitation studies of the diffuse bands of alkali metal dimers," *Journal of Chemical Physics,* vol. 88, pp. 2235-2241, 1988.

[20] Y. Takasu, K. Komori, K. Honda, M. Kumakura, T. Yabuzaki and Y. Takahashi, "Photoassociation Spectroscopy of Laser-Cooled Ytterbium Atoms," Physical Review Letters, vol. 93, no. 12, pp. 123202/1-4, 2004.

[21] J. K. Messer and F. C. De Lucia, "Measurement of Pressure-Broadening Parameters for the CO-He System at 4 K," Physical Review Letters, vol. 53, pp. 2555-2558, 1984.

[22] J. M. Doyle, B. Friedrich, J. Kim and D. Patterson, "Buffer-gas loading of atoms and molecules into a magnetic trap," Physical Review A, vol. 52, no. 4, pp. R2515-R2518, 1995.

[23] J. W. Dunn, D. Blume, B. Borea, B. E. Granger and C. H. Greene, "Feshbach Resonance Cooling of Trapped Atom Pairs," Physical Review A, vol. 71, no. 3-B, pp. 033402/1-033402/4, 2005.

[24] J. H. Blokland, J. Riedel, S. Putzke, B. G. Sartakov, G. C. Groenenboom and G. Meijer, "Producing translationally cold, ground-state CO molecules," Journal of Chemical Physics, vol. 135, pp. 114201 (1-6), 2011.

[25] M. S. Elioff, J. J. Valentini and D. W. Chandler, "Subkelvin Cooling NO Molecules via "Billiard-like" Collisions with Argon," Science, vol. 302, pp. 1940-1943, 2003.

[26] R. Levine, Molecular Reaction Dynamics, Cambridge, UK: Cambridge University Press, 2005.

[27] G. Scoles, Atomic and Molecular Beam Methods: Volume 1, New York: Oxford University Press Inc., 1988.

[28] K. T. Lorenz, M. S. Westley and D. W. Chandler, "Rotational state-to-state differential cross sections for the HCl-Ar collision system using velocity-mapped ion imaging," Physical Chemistry Chemical Physics, vol. 2, pp. 481-494, 2000.

[29] A. B. Eppink and D. H. Parker, "Velocity map imaging of ions and electrons using electrostatic lenses: Application in photoelectron and photofragment ion imaging of molecular oxygen," Rev. Sci. Instrum., vol. 68, no. 9, pp. 3477-3484, 1997.

[30] "Spectroscopy," Encyclopaedia Brittanica, 2012. [Online]. Available: http://www.britannica.com/EBchecked/topic/558901/spectroscopy. [Accessed 21 June 2012].

[31] C. H. Townes and A. L. Schawlow, Microwave Spectroscopy, Toronto, Ontario: McGraw-Hill Book Company, Inc., 1975.

[32] QMC Instruments Ltd., Test Data and Guarantee: InSb Detector Model QFI/X Low Noise Preamplifier Model ULN95, Cardiff, UK, 2010.

[33] Infrared Laboratories, "Winston Cones," 2010. [Online]. Available: http://www.infraredlaboratories.com/Winston_Cones.html. [Accessed 30 Juner 2012].

[34] NASA Jet Propulsion Laboratory, "Molecular Spectroscopy," [Online]. Available: http://spec.jpl.nasa.gov/. [Accessed 30 June 2012].

[35] G. B. Arfken and H. J. Weber, Mathematical Methods for Physicists, Fourth Edition, San Diego: Academic Press, Inc., 1995.

[36] B. Armstrong, "Spectrum Line Profiles: The Voigt Function," J. Quant. Spectrosc. Radiat. Transfer, vol. 7, pp. 61-88, 1967.

[37] D. A. McQuarrie and J. D. Simon, Physical Chemistry: A Molecular Approach, Sausalito, CA: University Science Books, 1997.

[38] H. M. Pickett, E. A. Cohen, B. J. Drouin and J. C. Pearson, *Submillimeter, Millimeter, and Microwave Spectral Line Catalog*, Jet Propulsion Laboratory: Molecular Spectroscopy, 2003.